Revision submitted to : *ACS Biomacromlecules*

In-Cell Association of a Bioorthogonal Tubulin

Yuhan Wang[1], Mahima Unnikrishnan[2], Brooke Ramsey[1], Driss El Andlosy[3], Alex T. Keeley[2], Catherine J. Murphy[2], and Martin Gruebele[1,2,4]

[1]Center for Biophysics and Quantitative Biology, University of Illinois Urbana-Champaign, Urbana, IL 61801, USA, [2]Department of Chemistry, University of Illinois Urbana-Champaign, Urbana, IL 61801, USA, [3]Computer Science and Technologies Department, Parkland Community College, Champaign, IL 61821, USA, [4]Department of Physics, University of Illinois Urbana-Champaign, Urbana, IL 61801, USA.

* Corresponding author: Martin Gruebele, mgruebel@illinois.edu

Abstract

Studies of proteins from one organism in another organism's cells have shown that such exogenous proteins stick more, pointing towards co-evolution of the cytoplasm and protein surface to minimize stickiness. Here we flip this question around by asking whether exogenous proteins can assemble efficiently into their target complex in a non-native cytoplasm. We use as our model system the assembly of BtubA and BtubB from *Prosthecobacter* hosted in human U-2 OS cells. BtubA and B evolved from eukaryotic tubulins after horizontal gene transfer, but they have low surface sequence identity with the homologous human tubulins, and do not respond to tubulin drugs such as nocodazole. In U-2 OS cells, BtubA and B assemble efficiently into dimers compared to *in vitro*, and the wild type BtubA and B proteins subsequently are able to form microtubules as well. We find that generic crowding effects (Ficoll 70 *in vitro*) contribute significantly to efficient dimer assembly when compared to sticking interactions (U-2 OS cell lysate *in vitro*), consistent with the notion that a generic mechanism such as crowding can be effective at driving assembly of exogenous proteins even when protein-cytoplasm quinary structure and sticking have been modified in a non-native cytoplasm. A simple Monte Carlo model of *in vitro* and in-cell interactions, treating BtubA and B as sticky dipoles in a matrix of sticky or non-sticky crowders rationalizes all the experimental trends with two adjustable parameters, and reveals nucleation as the likely mechanism, for the time-scale separation between dimer- and tubule-formation in-cell and *in vitro*.

Keywords: tubulin assembly, live cell microscopy, bioorthogonal system, Monte Carlo model

Introduction

Both in nature and in industry, proteins or their variants are found in environments that are very different from the native environment in which they were originally expressed. The gamut ranges from proteins shuttled to the extracellular surface to interact with a host, to enzymes engineered to function in non-aqueous solvents.[1,2] An interesting subclass of experiments has investigated how proteins behave in a non-native cytoplasm, such as a bacterial protein in a human cell, or vice-versa. Some important general findings are that such exogenous proteins generally stick more to other cytoplasm components, may be destabilized relative to native proteins, and that surface electrostatics is an important determinant of sticking.[3–7]

Much less studied are protein-protein interactions within non-native cellular environments. For example, Hsp70 heat shock protein will bind and protect yeast phosphoglycerate kinase in human cells, and protein GB1 homodimers are more stable in eukaryotic cells than in bacterial cells despite crowding being higher in bacterial cells .[8,9] Here we study the question of how heterodimer assembly and subsequent polymer formation is affected inside a non-native cytoplasm, and to what extent simulations and *in vitro* crowding and sticking control experiments can shed light on what factors hinder or promote assembly of exogenous complexes in a eukaryotic cytoplasm. We emphasize dimers as a first step and demonstrate time scale separation to polymer formation, enabling such studies in the future.

We quantify the interaction of prokaryotic tubulin proteins inside eukaryotic cells. Microtubules are key components of the eukaryotic cytoskeleton, supporting cell structure, transport, and division.[10–14] They are polymers made of 'AB' dimers of α-tubulin and β-tubulin[15] that assemble and disassemble dynamically.[16–18] Our model proteins are bacterial tubulins A and B (BtubA and B), from *Prosthecobacter*.[19–25] The Btub protein surfaces have evolved in bacterial cells, and hence are biorthogonal to human tubulins, with which they do not cross-assemble.[26] Btub proteins form 'AB' heterodimers that subsequently form protofilaments via the 'BA' interface assisted by GTP (physiological concentration ≈0.5 mM in human cells[27]), finally assembling into 4- to 5-bundle microtubule-like structures[19,21,23].

We begin with a non-tubule-forming mutant[21] of BtubA and B that forms 'AB' dimers only. Förster resonance energy transfer (FRET) microscopy detects dimers in-cell, while a simple Monte Carlo model consistent with experimental evidence for nucleation rules out a large concentration of oligomers. We find that the dissociation constant K_d of Btub dimerization is much smaller in human U-2 OS cells than in buffer. Past in-cell studies have concluded that in some cases, sticking to other macromolecules dominates protein-protein or protein-RNA interactions,[9,28] and in others, crowding is sufficient to account for association.[8,29] The crowding-sticking contribution remains an interesting mechanistic question and for BtubA and B, *in vitro* measurements support a significant contribution from crowding to the reduced K_d. This observation is consistent with the idea that a generic effect like crowding can promote assembly of an exogenous protein

complex even when quinary structure (stabilizing sticking)[30,31] has been disrupted by placing the complex in a non-native cytoplasm. We conclude that assembly of bioorthogonal exogenous protein dimers can be assisted significantly by a non-native cytoplasm compared to *in vitro*, and that crowding plays an important role in this particular case. We follow up these studies with similar measurements on the tubule-forming wild type of BtubA and B, and find that it can form tubular structures in eukaryotic cells (and *in vitro* in presence of GTP) on a time scale much longer than dimer assembly. Our Monte Carlo model indicates that nucleation of a Btub oligomer is the rate-limiting step that slows down tubule formation.

Materials and Methods

Plasmid design, protein expression and buffers Plasmids of BtubA and B were cloned and edited on the basis of the pDream2.1 vector (GenScript Biotech) with ampicillin resistance. For *in vitro* purification, a 6×His-tag and thrombin cleavage site were added to the N-terminus of the protein. See SI *Methods*, and SI **Table S1** for sequences. BL21 codon cells (Agilent) were transformed and cultured at 37 °C, then induced and incubated at 18 °C overnight. Cells were lysed and AKTA FPLC with a His-trap affinity chromatography column purified protein from filtered cell lysate. Elution buffer was made of 500 mM NaCl, 50 mM Na_3PO_4, 500 mM imidazole, pH=7.4. HMK buffer was 50 mM HEPES, 5 mM MgAc, 350 mM KAc, and 1 mM EGTA, pH=7.7 with KOH. KCl-based phosphate-buffered saline (PBS) buffer was 140 mM KCl, 10 mM K_2HPO_4, 1.8 mM KH_2PO_4, and pH 7.4. 150 mg/ml of Ficoll 70 (Sigma) or 1.0 mg/ml cell lysate (extracted from U-2 OS cells, see SI *Methods*) can be added to PBS buffer for certain *in vitro* conditions. Dissociation buffer was 500 mM KCl, 20 mM potassium phosphate, pH = 7.4. See SI *Methods* for further details.

Cell culture, microinjection, and imaging Human bone osteosarcoma (U-2 OS) cells were cultured in imaging dishes. Microinjection solution was prepared by mixing BtubA and B in the desired ratio in dissociation buffer and microinjected into individual cells. Cells were imaged through a ET470/40× bandpass filter (Chroma) with a T495lpxt dichroic to excite mEGFP and get FRET, and though a T580/25× bandpass filter and T600lpxr dichroic to direct excite mRuby3 for in-cell concentration calibration with a Zeiss, 63×/0.85 NA N-Achroplan objective. Emission passed through a ET500lp filter (Chroma) and was split into two channels using a T600lpxr dichroic (Chroma). For further details of confocal or electron microscopy, and U-2 OS cell lysate preparation, see SI *Methods*.

***In vitro* and in-cell data analysis** All data were analyzed using MATLAB. To quantify K_d of FRET-labeled BtubA and B, binding experiments were performed.

For in-cell experiments, the workflow in SI **Fig. S1** was used: A dish heater was used to maintain the temperature within ±1 degree (SI **Fig. S2**). Cells were co-injected with known concentrations of BtubA and BtubB, to fix the in-cell protein concentration ratio. The average cell height was measured by z-stack imaging using confocal microscopy (SI **Fig. S3**). Absolute in-cell concentrations of BtubB were then determined by comparing in-cell mRuby fluorescence excited directly with yellow light (SI **Fig. S4**) with that from a solution of known concentration and pathlength on the same instrument. The FRET signal due to fluorophores interacting with one another is negligible (SI **Fig. S5**), which also rules out unwanted background signal if there is a small amount of hydrolysis of the linker between Btub protein and fluorescent label. The FRET signals are plotted as a function of the green and red protein concentration. The 2-D surfaces are fit to Eq. (1), where F is the fluorescence signal, X (Y) is the concentration of green (red) protein, and a (scaling factor for red fluorescence to concentration) and K_d (dissociation constant) are the two parameters obtained from fitting.

$$\mathrm{F} = \frac{\mathrm{a}}{2}\left[(\mathrm{X} + \mathrm{Y} + K_d) - \sqrt{(\mathrm{X} + \mathrm{Y} + K_d)^2 - 4\mathrm{XY}}\right] \quad (1)$$

For individual cell images, only the cytoplasm area is cropped. For 1-D curve fitting, X in Eq. (1) represents the constant green-fluorescent protein concentration used in the titration.

In vitro experiments were performed on a 96-well plate scanning both BtubA and B concentrations from 2 to 24 μM, the approximate range covered by in-cell experiments. Bleed through of green fluorescence into the red FRET channel and direct excitation of mRuby by the blue light used to excite mEGFP was corrected for by using measurement of BtubA-only and BtubB-only solutions.

Monte Carlo Simulations. All simulations were coded and run using MATLAB. The interaction between different molecules followed the modified Lennard-Jones interparticle potential $\boldsymbol{U}(\vec{\boldsymbol{r}}_{\boldsymbol{ij}})$ that can be written as:

$$U(\vec{r}_{ij}) = 4\varepsilon_r\left(\frac{\rho_{ij}}{r_{ij}}\right)^{12} - 4H_{ij}\cdot\frac{\varepsilon_{BD}}{{r_{ij}}^2}(\vec{\mu}_i\cdot\vec{r}_{ij})\cdot(\vec{\mu}_j\cdot\vec{r}_{ij})\left(\frac{\rho_{ij}}{r_{ij}}\right)^{6} - 4\varepsilon_{ST}\left(\frac{\rho_{ij}}{r_{ij}}\right)^{6}, \quad (2)$$

where $\boldsymbol{r_{ij}} = |\vec{\boldsymbol{r}}_{\boldsymbol{ij}}|$ is the interparticle distance. The repulsive potential constant $\boldsymbol{\varepsilon_r}$ is always nonzero. For crowders interacting with any other particles only $\boldsymbol{\varepsilon_r}\neq 0$ and $\boldsymbol{\rho_{ij}}$ defines the interparticle repulsion distance. For stickers interacting with BtubA or B $\boldsymbol{\varepsilon_{ST}}\neq 0$, resulting in an isotropic Lennard Jones potential. For BtubA and B interacting, the vector $\vec{\boldsymbol{\mu}}_{\boldsymbol{i}}$ points along the dimerization axis of BtubA or B and $\boldsymbol{\varepsilon_{BD}}\neq 0$, resulting in an anisotropic potential. $\boldsymbol{H_{ij}} = \pm 1$ differentiates the non-tubule mutant from wild type by inhibiting 'BA' dimer formation when $\boldsymbol{H_{ij}} = -1$, and allowing both BA and AB dimer formation when $\boldsymbol{H_{ij}} = 1$ (see SI **Fig. S6**). The anisotropic interaction promotes the formation of tubule-like structures from BtubA and B wild type in our model. The attractive well depth $\boldsymbol{\varepsilon_{BD}}$ was adjusted to match the *in vitro* buffer value of K_d for

mutant and wild type. $\boldsymbol{\varepsilon_{BD} = \varepsilon_r}$ were then held constant for all other simulations that add stickers or crowders to the system to see how well those trends are reproduced by the model when only the single parameter $\boldsymbol{\varepsilon_{ST}}$ is adjusted. SI **Fig. S7** and **Table S2** show the potential energy parameters and size parameters that were used for the simulation.

Molecules underwent Brownian motion in translation and rotation. Both the translational and rotational diffusion coefficient D of the molecules were defined (see SI *Methods*). For each sampling step, a potential movement based on Brownian motion (distance taken from a Gaussian distribution with root-mean-square width $\Delta x^2=6D\Delta t$ and random orientation) is proposed on a random-selected particle. Metropolis sampling is used to accept or reject the move based on the change in energy computed from Eq. (2). The sampling is continued until the total potential energy reaches equilibrium. The *in silico* dissociation constant $K_{d(in\ silico)}$ can be obtained from the equilibrium concentrations of protein monomers and dimers. Simulations initialized with either all monomers, half dimers, or all dimers equilibrated to the same K_d (SI **Fig. S8**). To simulate more complicated scenarios, one more molecule (light purple) is added to the system as the crowder to simulate purely repulsive volume exclusion, or stickers to simulate nonspecific sticking at lower crowder concentration. See SI **Table S3** for diffusion coefficients, and SI *Methods* for detailed accepting/rejection rules and potential settings.

Results and Discussion

Bioorthogonality of Btub proteins. We chose Btub proteins because their surface sequence identity with mammalian tubulin is less than 30% (SI **Table S4**),[32] making them likely to be biorthogonal to human tubulins: Unlike human tubulins, Btub A and B form 4- (*in vitro*) or 5- (*in vivo*) stranded tubules instead of 13-stranded microtubules.[23] Furthermore, multiple measurements failed to detect any stable association between BtubA or BtubB with any eukaryotic tubulin subfamily.[26] Finally, we performed experiments attempting to disrupt Btub tubules using the drug nocodazole, which is highly effective at disrupting eukaryotic tubule formation. Btub tubule formation is suppressed much less effectively by nocodazole than tubulin formation, as seen by TEM (SI **Fig. S9**). All of these observations point to a high degree of biorthogonality between prokaryotic BtubA and B and eukaryotic tubulin α and β.

FRET-labeled mutant BtubA and B dimerize *in vitro.* For our in-cell studies, we FRET-labeled BtubA and B so we can detect in-cell dimer formation ratiometrically via fluorescence color change. Furthermore, to avoid complications from polymerization, we initially studied a Btub mutant pair that forms the 'AB' dimer efficiently (small K_d), but cannot dimerize at the 'BA' interface, so it does not further

assemble into oligomers or microtubules.[21] Point mutations BtubA V179K and BtubB D249K disrupt the interface between dimers (**Fig. 1a**) by changing the charge and size of the amino acids.

We labeled mutant BtubA (mEGFP at C-terminus) and BtubB (mRuby3 at C-terminus) for FRET-detection of 'AB' dimer formation (**Fig. 1a**). To reduce the volume occupancy of the fluorophores at the interaction surfaces, we added a 15-amino-acid Gly-Gly-Ser repeat linker between each protein and fluorophore. The distance between the fluorophore pairs within the 'AB' heterodimer is <4 nm, giving a high calculated FRET efficiency >90% (SI **Fig. S10**). The distance between the fluorophores in other configurations (e.g., across the 'BA' interface) is >10 nm, with a low calculated FRET efficiency <5%.

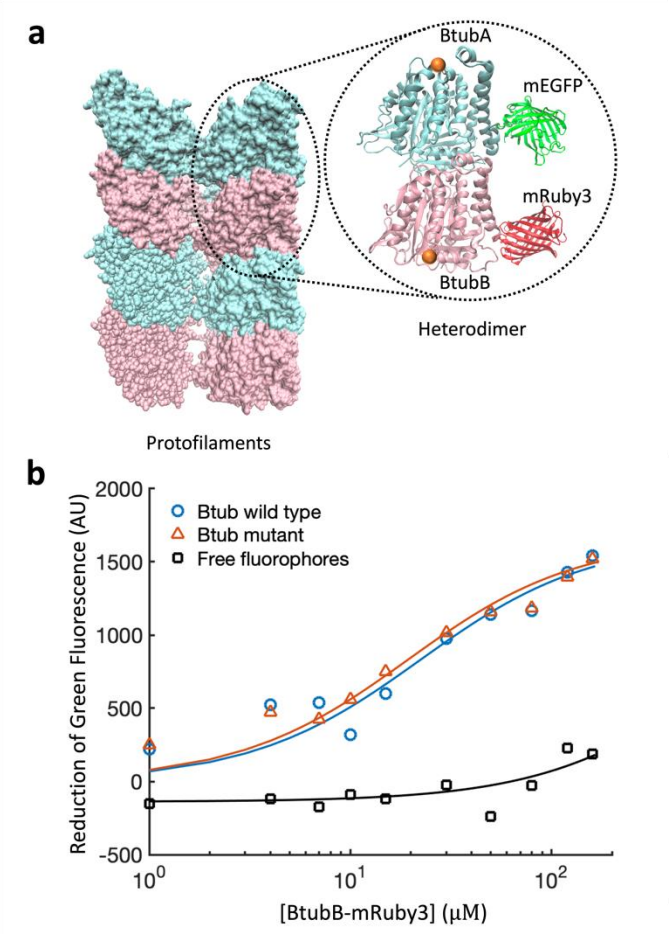

Fig. 1. FRET-labeled BtubA and BtubB and their binding titration curve *in vitro*. (a) BtubA and B protofilaments (left, PDB: 5o09) and heterodimer (right, PDB: 2btq). mEGFP is labeled on the C terminus of BtubA and mRuby3 is labeled on the C terminus of BtubB. Point mutation sites at the 'BA' dimer surface to make the non-tubule-forming mutant are at orange spheres. (b) The reduction of green fluorescence due to FRET monitors the binding titration of FRET-labeled BtubA and B mutant (orange) and wild type (blue) in HMK buffer. Such traces can be obtained within a few minutes due to rapid dimerization of wild type and mutant. The concentration of the green protein is 2 μM. Excitation: 450 nm, Emission: 490-700 nm. See SI **Fig. S11** for full spectra.

In **Fig. 1b**, we compare the K_d of our mutant pair with the wild type (fluorescence traces are shown in SI **Fig. S11**). In HMK buffer (see *Methods*), a model for bacterial cell ionic strength, K_d of our mutant FRET pair is 18±4 μM at 22 °C compared to the wild type K_d of 21±4 μM, so the non-tubule point mutation does not substantially affect dimerization. The fluorophores mEGFP and mRuby3 by themselves do not show any measurable assembly over the 1 to 160 μM range (Fig. 1b). We also swapped fluorophores on BtubA and B, yielding K_d = 36±7 μM at 22 °C (SI **Fig. S12**), and thus performed subsequent experiments with the higher affinity pair.

FRET-labeled mutant BtubA and B do not form tubules *in vitro*. To verify that our FRET-labeled mutants do not form protofilaments or microtubules, as previously reported for the unlabeled Btub mutants in the literature,[19] we compared its transmission electron microscopy (TEM) with wild type BtubA and B, both in in 1:1 mixtures. Unlike wild type, the FRET-labeled mutant forms no discernible microtubules in either PBS or HMK buffer (**Fig. 2** and SI **Fig. S13**). Thus, the mutant isolates dimerization from polymerization *in vitro*. PBS buffer with 0.5 mM GTP, close to the reported concentration in human cells,[27] (see *Methods*), was used in all subsequent *in vitro* experiments as a model for human cell ionic strength for comparison with the U-2 OS cytoplasm. Note that wild type assembly into microtubules, as discussed further below, occurs on a longer time scale than our dimerization measurements *in vitro* or in-cell.

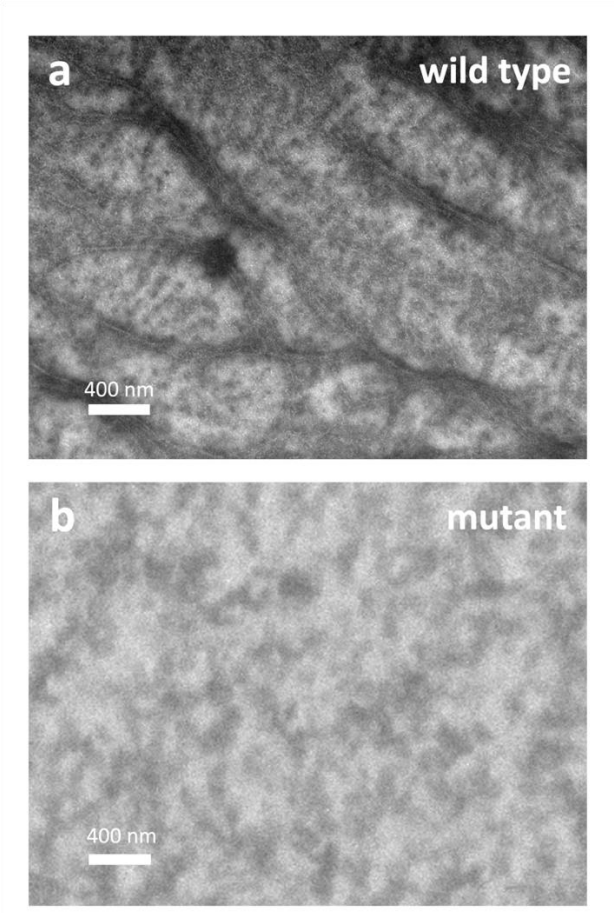

Fig. 2. The assembly of FRET-labeled BtubA and B under transmission electron microscopy (TEM). (a) A mixture of wild type BtubA-mEGFP and BtubB-mRuby3 (5 μM each) forms microtubules in PBS buffer. (b) A mixture of non-tubule mutant BtubA-mEGFP and BtubB-mRuby3 (5 μM each) does not form tubules in PBS buffer. All samples were prepared with 0.5 mM GTP and stained using 0.2 % ammonium molybdate (see SI *Methods*). The scale bars are 400 nm.

The cytoplasm promotes Btub dimerization equilibrium by an order of magnitude over dilute buffer. Next, we studied our core question: does a eukaryotic cytoplasm, here in human U-2 OS cells, promote formation of exogenous bacterial BtubA and B heterodimers compared to *in vitro*? Any difference between K_d in cells and in buffer arises from differences in these environments. Btub proteins in-cell are subject to both macromolecular crowding (repulsive interactions) and sticking (attractive interactions with other macromolecules modulated by metabolites and ions). Generally, one expects that crowding increases association due to the smaller available free volume, whereas sticking could go either way[9,28,33,34] by competing with complex formation, or by stabilizing the complex through favorable interactions. Crowding is a very generic volume exclusion effect, whereas favorable sticking (so-called quinary interactions) [30,31] must co-evolve between a dimer surface and its host cytoplasm.[5,31]

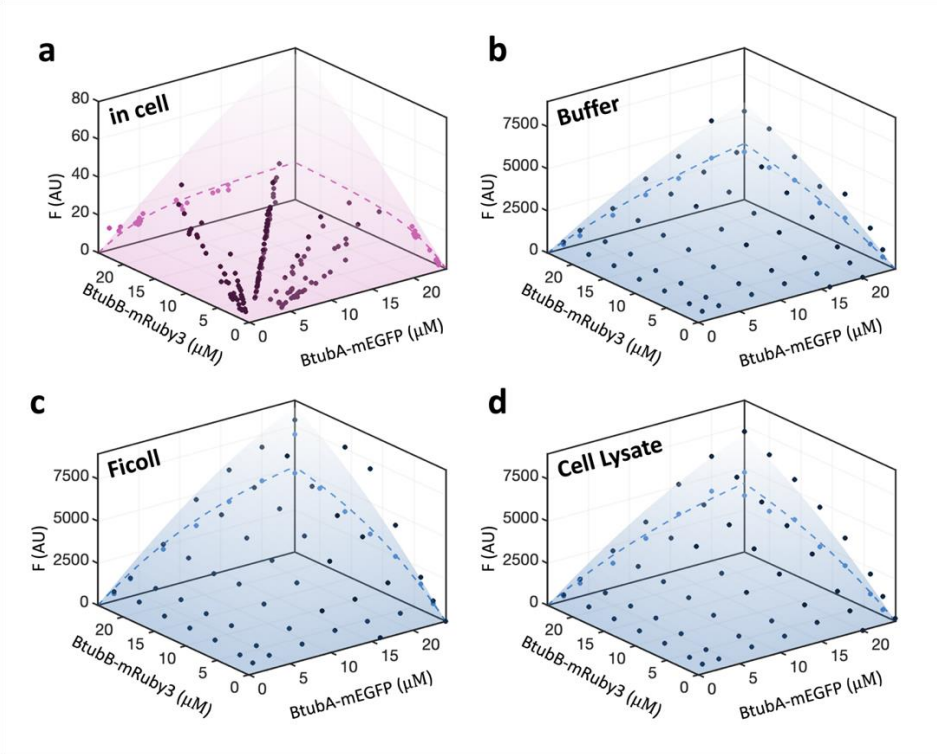

Fig. 3. 2D-surface fitting of non-tubule BtubA and B binding experiments in cell (pink) and *in vitro* (blue). (a) Fitting in-cell measurements with a 2-D binding surface to obtain dissociation constant K_d of non-tubule mutant BtubA and B. The FRET signal increases as a function of in-cell FRET-BtubA and B concentration. Each dot represents an individual cell microinjected with a BtubA and B mixture of known A:B concentration ratios (BtubA:BtubB = 1:1, 1:2, 1:3, 1:4, 4:1, 3:1, 2:1). The intensities of cells containing 7±1 μM BtubB-mRuby3 are projected onto the left back plane (pink dots on the plane) and can be fitted by 1-D binding curve (pink dotted curve). The intensities of cells containing 7±1μM BtubA-mEGFP are projected to right back plane (pink dots on the plane) to show a 1-D binding curve (pink dotted curve). The entire set of data was fitted by a 2-D surface using Eq. (1). (b) 2-D binding surface for *in vitro* data in PBS buffer with 0.5 mM GTP, (c) with 38% vol. crowder (150 mg/ml Ficoll 70) and (d) with 1.0 mg/ml cell lysate. Each dark blue dot is extracted from an individual spectrum with a known BtubA and B concentration (grid of 0, 2, 4, 8, 12, 16, 20, 24 μM). The data points with 12 μM BtubB-mRuby3/BtubA-mEGFP are projected onto left/right back plane to show 1-D binding curves (blue dotted curve). The entire set of data is fitted by a 2-D surface using Eq. (1).

Experiments to determine K_d in four cases (in-cell, PBS buffer, Ficoll, and lysate) were performed by 2-D scans of mutant BtubA and B concentrations, (**Fig. 3** and *Methods*, full data in SI **Fig. S15**), and fitted to Eq. (1) to obtain K_d (**Fig. 4**). In U-2 OS cells at 22 °C, K_d = 2.4±0.6 μM is a factor of 10 smaller than in PBS buffer, which corresponds to a 10-fold increase of the binding affinity. A lesser but still significant decrease in-cell is observed at 37 °C. Thus, eukaryotic cells strongly promote assembly of prokaryotic Btub dimer when compared to PBS buffer with GTP.

To dissect the effect of crowding and sticking on dimer formation *in vitro*, we performed control experiments in the 70 kDa crowder Ficoll 70 and in two concentrations of dilute U-2 OS cell lysate. 150 mg/ml Ficoll 70 reduces K_d from 24 to 5±1 μM at 150 mg/ml relative to buffer. At this concentration, Ficoll has a hydrodynamic swollen polymer occupancy of ≈ 38%,[35] although some estimates of hydrodynamic

radius and occupancy are even larger.[36–38] Thus, Btub association in the Ficoll crowder comes within a factor of 2 of the in-cell K_d at a significantly lower volume occupancy of crowder than in-cell (≈ 280 mg/ml macromolecules in eukaryotic cells, higher in bacteria[34,39–42]). The stabilizing effect of *in vitro* crowding is less pronounced at 37 °C, but persists. In all experiments, K_d increases at 37 °C relative to 22 °C, so the dissociation reaction is endothermic, and thus must rely on entropic effects to drive the reaction.

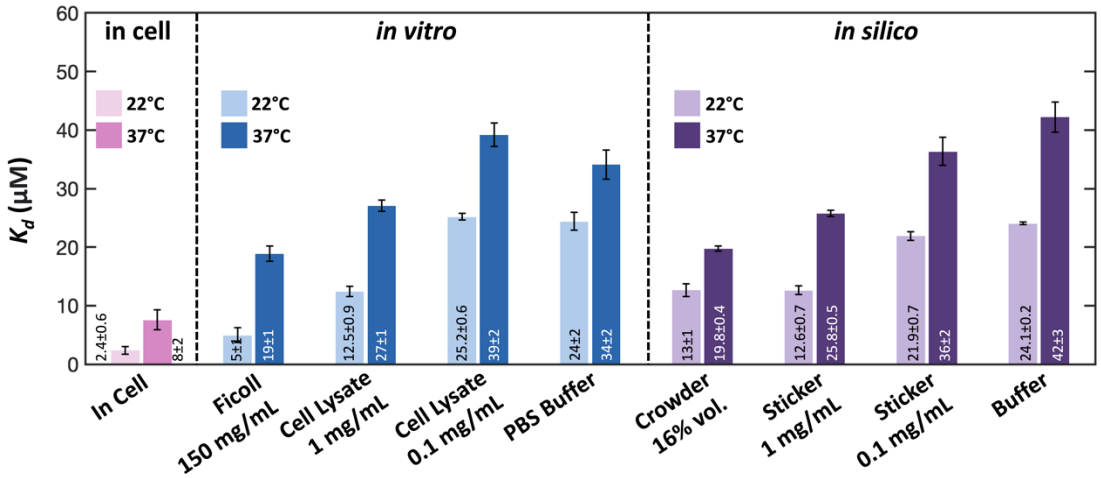

Fig. 4. The binding affinities of non-tubule mutant BtubA and B in-cell (pink), *in vitro* (blue), and from simulations (purple) at 22 and 37 °C. The dissociation constant K_d was obtained by fitting Eq. (1) to the data in SI **Fig. S15**. Numerical values are shown and plotted in a bar chart to visualize the differences between in-cell, *in vitro* crowding (150 mg/ml Ficoll 70, 38% by vol.), sticking to cell lysate (0.1 mg/ml and 1 mg/ml), PBS buffer, and simulation described in the text (16% by vol. crowders, 0.1 mg/ml and 1 mg/ml stickers, and BtubA and B only as 'buffer'). 166 cells were measured at 22°C, and 71 cells at 37 °C. The in-cell error bars were determined from global fitting among cells. 96 different concentrations were measured to obtain one readout of the K_d value and the error bars show one standard error from three K_d readouts *in vitro* and *in silico*. Data values are also provided in SI **Table S5**.

In contrast, the most dilute lysate (0.1 mg/ml,), in which crowding plays no role, either slightly increases K_d (37 °C) or has no noticeable effect (22 °C). (We observe an even more pronounced destabilizing trend in lysate for the wild type dimer, discussed below.) In 1 mg/ml lysate, where crowding begins to contribute[43] and sticking partners are in excess compared to Btub A and B, less stabilization is observed than in Ficoll. Membrane interactions do not contribute either: analysis of small, evenly fluorescent cytoplasm sections produce the same K_d as whole-cytoplasm averages, so Btub dimerization was uniform throughout the cytoplasm (SI **Fig. S14**). Thus we conclude that at least *in vitro*, crowding makes a significant contribution to stabilizing the Btub dimer when compared to sticking.

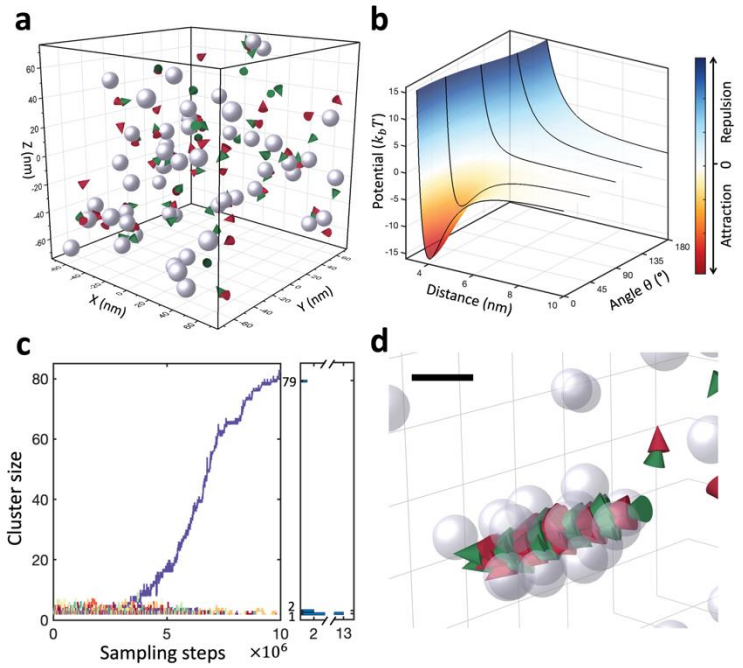

Fig. 5. Monte Carlo-based simulation of BtubA and B dimerization and tubule formation. (a) The simulation system is illustrated for 24 μM mutant BtubA and BtubB (green and red cones pointing along $\vec{\boldsymbol{\mu}}$, 48 molecules each) in the presence of 'stickers/crowders' (spheres). The simulation box is 150 nm on each side. If a simulation step is interpreted as 100 ns long the proteins diffuse with D = 108 μm^2/s in buffer. Simulations under different conditions see SI **Fig. S16**. (b) Potential energy in Eq. (2) between BtubA and BtubB molecules as a function of center-of-mass distance and angle θ between molecular directions $\vec{\boldsymbol{\mu}}$. SI **Fig. S7** shows the interaction potentials for all pairwise particle combinations. (c) Tubule lag phase kinetics when wild type BtubA and B form rudimentary microtubules with 1 mg/ml stickers. Clusters with $3 \leq n \leq 8$ are very rare as seen in the histogram on the right. (d) Snapshot of the tubule in (c). Scale bar is 20 nm. Other tubule formation simulation results are in SI **Fig. S17**.

The Btub dimerization trends are reproduced by a Monte Carlo model.

Our experimental results can be rationalized by a coarse-grained physics-based model simpler than all-atom simulations, but more detailed than empirical thermodynamic fitting. In our model, there are up to four types of diffusing particles: BtubA, BtubB, crowders, and stickers (**Fig. 5a**) that interact via the Lennard-Jones potential in Eq. (2) (See *Methods*). Crowders have only a repulsive potential interaction with each other and the Btub proteins. Stickers also have an attractive interaction with Btub proteins. Model mutant BtubA and B can form AB dimers via an anisotropic interaction (Eq. (1) in *Methods* and **Fig. 5b**), but they cannot form BA contacts or higher oligomers. Monte Carlo sampling of Brownian dynamics rotational and translational diffusion biased by the potential U (see *Methods*) equilibrates the system. The sampling steps are not-time steps, but the Brownian rotation/diffusion move set of the simulations resembles dynamics enough, so one can think of a sampling step as corresponding to about 100 ns in real time. We represent all energies in k_BT units (T = 295.15 K), so temperature is implicitly included in the model.

Simulations were run with multiple concentrations of BtubA and B in triplicate until concentrations reached a steady state to obtain *in silico* 2-D binding surfaces (SI **Fig. S15**). The attractive Lennard-Jones parameter ε_{BD} was fitted to reproduce the K_d in buffer at 22 °C (**Fig. 4**) and held constant in all further simulations. The simulations also reproduced the 'sticking' at 22 °C by adding 1 mg/ml sticker with one more independent parameter, the sticker-Btub interaction strength ε_{ST}=6.5 k_BT. Without further adjustment, the K_d in **Fig. 4** were obtained for 16% by volume crowder, 0.1 mg/ml sticker, and for all conditions at 37 °C. The simulations converged too slowly at the experimental crowder volume fraction of ≥38%, so K_d at 16% in **Fig. 4** is an upper limit on the 150 mg/ml Ficoll experiment, consistent with the experimental data.

The model reproduces the trends seen in all experiments in **Fig. 4** by using just two adjustable parameters, with the exception of the 0.1 mg/ml cell lysate data, which yielded an increased K_d in experiment relative to buffer, indicating that sticking under low-crowding conditions either speeds up the dissociation reaction by reducing stability of the dimer, or slows down the association reaction by occupying the BtubA and B binding surfaces. Thus, our simulations support the observation that crowding *in vitro* makes a contribution larger than sticking towards decreasing K_d of BtubA and B.

Wild type Btub forms tubules with a lag phase in the Monte Carlo model and in human cells

We also carried out experiments *in vitro* and in-cell with wild type BtubA and B, which can form microtubule-like structures after forming dimers. **Fig. 6** shows the growth of Btub microtubules in U-2 OS cells imaged by confocal fluorescence microscopy. 40 minutes after injection of BtubA and B in a 3:1 ratio to drive the equilibrium towards association while minimizing background in the red fluorescence channel, the automated SOAX algorithm for detecting tubules[44] shows no significant signal for the mutant (**Fig. 6a** and **b**), but formation of multiple long tubules for the wild type (**Fig. 6c** and **d**). The proteins do not accumulate in the cell nucleus, hence the contrast in **Fig. 6d** is best in the thin cytosol layer (~1 μm)[41] above and below the nucleus where the background fluorescence from monomers and dimers is smaller. Importantly, there is a lag phase for tubule formation from the wild type proteins, such that dimerization can be measured separately in experiments carried out in < 30 minutes (SI **Fig. S19**). **Fig. 6** also shows that mutant and wild type Btub proteins do not discernibly interact with membranes in-cell or disrupt cell shape, another indication of the orthogonality of the bacterial Btub system to human tubulins.

Thus we were able to study the wild type dimer equilibrium in-cell and *in vitro* as well, using the same protocols described for the mutant earlier, by collecting data in < 30 minutes. The resulting K_d values are shown in SI **Fig. S20**. The results follow similar trends as for the mutant, but cell lysate destabilizes the wild type dimer even more as compared to the mutant, whereas crowding is not as effective at promoting dimerization at the higher temperature (37 °C).

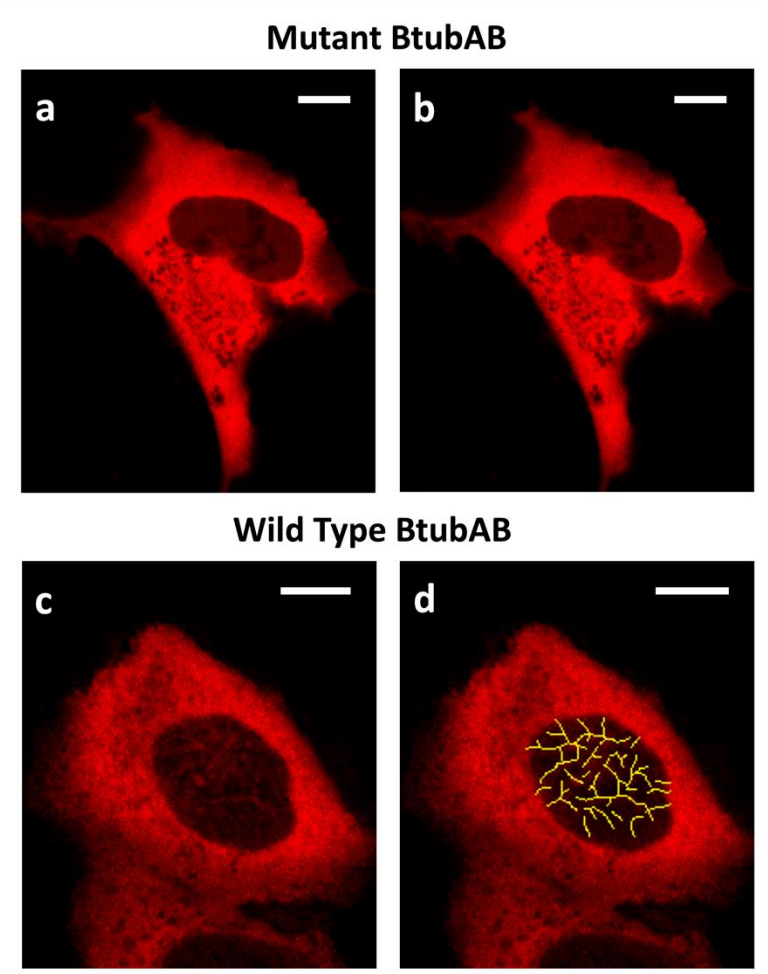

Fig. 6. Images of BtubA and B in U-2 OS cells under a confocal microscope. (a) Non-tubule-forming mutant BtubA (120 μM) and BtubB (40 μM) mixture injected and imaged under a LSM 880 confocal microscope; excitation: 581 nm; emission: 590-650 nm. (b) SOAX software is not able to detect microtubules in the thin area of cytoplasm above and below the nucleus where contrast is best, indicating absence of detectable microtubules. (c) FRET-labeled wild type BtubA and B imaged in the red channel form microtubules in a U-2 OS cell. The microtubules are visible in the thinner cytoplasm area below and above the nucleus. Excitation: 581 nm. Emission: 590-650 nm. (d) Microtubule structures from (c) are auto-identified and highlighted in yellow using SOAX software. Scale bars are 10 μm. For control experiment with only injecting BtubA or BtubB, see SI **Fig. S18**.

The Monte Carlo model also reproduced the trends observed experimentally for the wild type. With the 'BA' interaction turned on to simulate the wild type (see *Methods*), lowering ε_{ST} from 6.5 to 4.0 k_BT eliminates the effect of sticking on K_d (SI **Fig. S20** and **Table S2**), as observed experimentally. The simulations explain why tubule growth is delayed for the wild type, thus enabling dimerization equilibrium measurements. Figs. **5c** and **d** illustrates the formation of elongated tubules in our model (see SI **Fig. S16-17** for additional conditions). Delayed nucleation of tubules occurs only when ≥4 BtubA and B dimers have assembled into a small cluster (**Fig. 5c**); as can be seen from the histogram in **Fig. 5c**, the average

concentration of trimers and higher oligomers remains small compared to the concentration of monomers, dimers, and tubules, explaining why Eq. (2) in *Methods* works well when fitting the data.

Conclusions

While it has been possible to quantify the dimerization equilibrium of eukaryotic tubulins *in vitro*, it has proven difficult inside live cells, due to the perturbation of the cell by cytoskeletal drugs or initiators. The bioorthogonal Btub proteins, evolved in bacteria after horizontal gene transfer from eukaryotes, solve this problem. Evolution of the proteins' surfaces could be responsible for the apparently weak interaction of Btub proteins with α- and β-tubulin[20]: BtubA and B have up to 39% sequence identity to human α- and β-tubulins[32], but for the surface residues it is only up to 29% (SI **Table S4**).

Using FRET, we were able to show that a dimer-only mutant dimerizes 10 times more effectively inside U-2 OS cells than in a GTP-containing buffer of ionic strength similar to that of the cytoplasm. More than electrostatics play a role in modulating binding in-cell: the dissociation reaction is endothermic in all media, indicating that an entropic driving force plays a role. In our *in vitro* controls, macromolecular crowding by Ficoll enhances dimer formation more than macromolecular sticking by an excess of U-2 OS cell lysate, whereas wild type dimer association is even reduced in cell lysate when compared to buffer. We see no evidence of increased association at membranes. Thus, crowding is a good candidate for enhanced Btub association in-cell. We see yet again that crowding and sticking are sufficiently balanced such that either can contribute significantly in-cell, depending on the details of the macromolecular system in question.[9,28,33,34,45] For Btub proteins, it is perhaps not entirely surprising that cell-specific interactions are less important than generic crowding compared to some other proteins: these proteins are bioorthoogonal to mammalian cells, and their surfaces have likely, in bacteria, evolved away from enabling favorable quinary structure in mammalian cells.

Adjustment of two parameters in a simple anisotropic binding potential matches the *in vitro* buffer value of K_d, and reproduces the observed trends in K_d when modeling Ficoll 70 as a repulsive crowder, and cell lysate as dilute 'stickers' (SI **Table S2**). The model shows that dimerization of wild type is consistent with a weaker sticking interaction compared to the mutant (4.5 vs. 6.5 k_BT). While dimerization occurs after a few simulation steps, the model also shows that oligomers other than dimers are rare, leading to nucleation kinetics for the formation of microtubules. Microtubule formation, such as seen in **Fig. 5d** (simulation) takes much longer than the rapid dimerization reaction. This time delay for tubule formation, as we observed in-cell in **Fig. 6c**, allows dimerization and tubule formation can be studied conveniently on separate time scales.

The real in-cell situation is clearly not as simple as our *in vitro* controls or simulations: the in-cell enhancement of dimer formation remains sub-10 μM at 37 °C, whereas both *in vitro* experiments and our model with two adjustable parameters predict a smaller relative temperature effect than observed in-cell This shows that in the cell, entropic effects that favor dissociation at higher temperature are not alone responsible for enhanced dimer formation, but that enthalpic effects also play a role. Indeed, the role of enthalpy in crowding has been revealed recently.[46] Thus, even crowding-based models need to take entropy-enthalpy compensation into account to quantitatively explain why binding is so highly enhanced in-cell at room temperature. In our model, this could be achieved via a temperature-dependent interaction potential ε_{ST} in Eq. (1). The origin of this compensation effect remains to be explained, but we propose the following testable hypothesis for future experiments: The Debye-Hückel screening length depends strongly on the dielectric constant of the solvent, causing reduced electrostatic interaction at higher temperature in aqueous solution.[47] In contrast, the hydrophobic interaction strength increases with temperature,[48] so better water exclusion from hydrophobic protein patches that interact in-cell counteracts the weakening of electrostatic interactions.

Supporting Information

The supporting information PDF file contains a schematic workflow for in-cell K_d measurements, additional spectra, control experiments, definition of parameters and potentials used in the simulation, and supplementary experimental and computational methods.

Acknowledgments

This work was supported by the National Science Foundation (NSF) Grant NSF MCB 2205665 (M.G., Y.W. and M.U.) This work was also supported by the National Science Foundation under Grant No. CHE-2001611, the NSF Center for Sustainable Nanotechnology (C.J.M and M.U.). We thank Materials Research Laboratory staff scientists Lou Ann Miller and Dr. Kristen Flatt for their help with TEM imaging. We thank Core Facility staff scientist Dr. Austin Joseph Cyphersmith for his help with LSM880 confocal imaging. We thank Prof. Jan Löwe at Medical Research Council Laboratory of Molecular Biology, Cambridge, UK, for kindly offering the plasmids of BtubA and B.

References

(1) Samiotakis, A.; Wittung-Stafshede, P.; Cheung, M. Folding, Stability and Shape of Proteins in Crowded Environments: Experimental and Computational Approaches. *Int. J. Mol. Sci.* **2009**, *10* (2), 572–588. https://doi.org/10.3390/ijms10020572.

(2) Arnold, F. Engineering Enzymes for Non-Aqueous Solvents. *Trends Biotechnol.* **1990**, *8*, 244–249. https://doi.org/10.1016/0167-7799(90)90186-2.

(3) Guzman, I.; Gelman, H.; Tai, J.; Gruebele, M. The Extracellular Protein VlsE Is Destabilized inside Cells. *J. Mol. Biol.* **2014**, *426* (1), 11–20. https://doi.org/10.1016/j.jmb.2013.08.024.

(4) Leeb, S.; Sörensen, T.; Yang, F.; Mu, X.; Oliveberg, M.; Danielsson, J. Diffusive Protein Interactions in Human versus Bacterial Cells. *Curr. Res. Struct. Biol.* **2020**, *2*, 68–78. https://doi.org/10.1016/j.crstbi.2020.04.002.

(5) Gruebele, M.; Pielak, G. J. Dynamical Spectroscopy and Microscopy of Proteins in Cells. *Curr. Opin. Struct. Biol.* **2021**, *70*, 1–7. https://doi.org/10.1016/j.sbi.2021.02.001.

(6) Mu, X.; Choi, S.; Lang, L.; Mowray, D.; Dokholyan, N. V.; Danielsson, J.; Oliveberg, M. Physicochemical Code for Quinary Protein Interactions in Escherichia Coli. *Proc. Natl. Acad. Sci.* **2017**, *114* (23), E4556–E4563. https://doi.org/10.1073/pnas.1621227114.

(7) Cohen, R. D.; Pielak, G. J. Electrostatic Contributions to Protein Quinary Structure. *J. Am. Chem. Soc.* **2016**, *138* (40), 13139–13142. https://doi.org/10.1021/jacs.6b07323.

(8) Guin, D.; Gruebele, M. Chaperones Hsc70 and Hsp70 Bind to the Protein PGK Differently inside Living Cells. *J. Phys. Chem. B* **2020**, *124* (18), 3629–3635. https://doi.org/10.1021/acs.jpcb.0c00519.

(9) Speer, S. L.; Zheng, W.; Jiang, X.; Chu, I.-T.; Guseman, A. J.; Liu, M.; Pielak, G. J.; Li, C. The Intracellular Environment Affects Protein–Protein Interactions. *Proc. Natl. Acad. Sci.* **2021**, *118* (11), e2019918118. https://doi.org/10.1073/pnas.2019918118.

(10) Janke, C.; Magiera, M. M. The Tubulin Code and Its Role in Controlling Microtubule Properties and Functions. *Nat. Rev. Mol. Cell Biol.* **2020**, *21* (6), 307–326. https://doi.org/10.1038/s41580-020-0214-3.

(11) Vicente, J. J.; Wordeman, L. The Quantification and Regulation of Microtubule Dynamics in the Mitotic Spindle. *Curr. Opin. Cell Biol.* **2019**, *60*, 36–43. https://doi.org/10.1016/j.ceb.2019.03.017.

(12) Gudimchuk, N. B.; McIntosh, J. R. Regulation of Microtubule Dynamics, Mechanics and Function through the Growing Tip. *Nat. Rev. Mol. Cell Biol.* **2021**, *22* (12), 777–795. https://doi.org/10.1038/s41580-021-00399-x.

(13) Goodson, H. V.; Jonasson, E. M. Microtubules and Microtubule-Associated Proteins. *Cold Spring Harb. Perspect. Biol.* **2018**, *10* (6), a022608. https://doi.org/10.1101/cshperspect.a022608.

(14) Kirschner, M. W.; Mitchison, T. Microtubule Dynamics. *Nature* **1986**, *324* (6098), 621. https://doi.org/10.1038/324621a0.

(15) Alushin, G. M.; Lander, G. C.; Kellogg, E. H.; Zhang, R.; Baker, D.; Nogales, E. High-Resolution Microtubule Structures Reveal the Structural Transitions in Aβ-Tubulin upon GTP Hydrolysis. *Cell* **2014**, *157* (5), 1117–1129. https://doi.org/10.1016/j.cell.2014.03.053.

(16) Brouhard, G. J.; Rice, L. M. Microtubule Dynamics: An Interplay of Biochemistry and Mechanics. *Nat. Rev. Mol. Cell Biol.* **2018**, *19* (7), 451–463. https://doi.org/10.1038/s41580-018-0009-y.

(17) Akhmanova, A.; Steinmetz, M. O. Control of Microtubule Organization and Dynamics: Two Ends in the Limelight. *Nat. Rev. Mol. Cell Biol.* **2015**, *16* (12), 711–726. https://doi.org/10.1038/nrm4084.

(18) Gudimchuk, N. B.; Ulyanov, E. V.; O'Toole, E.; Page, C. L.; Vinogradov, D. S.; Morgan, G.; Li, G.; Moore, J. K.; Szczesna, E.; Roll-Mecak, A.; Ataullakhanov, F. I.; Richard McIntosh, J. Mechanisms of Microtubule Dynamics and Force Generation Examined with Computational Modeling and Electron Cryotomography. *Nat. Commun.* **2020**, *11* (1), 3765. https://doi.org/10.1038/s41467-020-17553-2.

(19) Sontag, C. A.; Staley, J. T.; Erickson, H. P. In Vitro Assembly and GTP Hydrolysis by Bacterial Tubulins BtubA and BtubB. *J. Cell Biol.* **2005**, *169* (2), 233–238. https://doi.org/10.1083/jcb.200410027.

(20) Schlieper, D.; Oliva, M. A.; Andreu, J. M.; Löwe, J. Structure of Bacterial Tubulin BtubA/B: Evidence for Horizontal Gene Transfer. *Proc. Natl. Acad. Sci. U. S. A.* **2005**, *102* (26), 9170–9175. https://doi.org/10.1073/pnas.0502859102.

(21) Sontag, C. A.; Sage, H.; Erickson, H. P. BtubA-BtubB Heterodimer Is an Essential Intermediate in Protofilament Assembly. *PLOS ONE* **2009**, *4* (9), e7253. https://doi.org/10.1371/journal.pone.0007253.

(22) Andreu, J. M.; Oliva, M. A. Purification and Assembly of Bacterial Tubulin BtubA/B and Constructs Bearing Eukaryotic Tubulin Sequences. *Methods Cell Biol.* **2013**, *115*, 269–281. https://doi.org/10.1016/B978-0-12-407757-7.00017-7.

(23) Deng, X.; Fink, G.; Bharat, T. A. M.; He, S.; Kureisaite-Ciziene, D.; Löwe, J. Four-Stranded Mini Microtubules Formed by *Prosthecobacter* BtubAB Show Dynamic Instability. *Proc. Natl. Acad. Sci.* **2017**, *114* (29), 5950-5958. https://doi.org/10.1073/pnas.1705062114.

(24) Díaz-Celis, C.; Risca, V. I.; Hurtado, F.; Polka, J. K.; Hansen, S. D.; Maturana, D.; Lagos, R.; Mullins, R. D.; Monasterio, O. Bacterial Tubulins A and B Exhibit Polarized Growth, Mixed-Polarity Bundling, and Destabilization by GTP Hydrolysis. *J. Bacteriol.* **2017**, *199* (19), e00211-17. https://doi.org/10.1128/JB.00211-17.

(25) Jenkins, C.; Samudrala, R.; Anderson, I.; Hedlund, B. P.; Petroni, G.; Michailova, N.; Pinel, N.; Overbeek, R.; Rosati, G.; Staley, J. T. Genes for the Cytoskeletal Protein Tubulin in the Bacterial Genus *Prosthecobacter*. *Proc. Natl. Acad. Sci.* **2002**, *99* (26), 17049–17054. https://doi.org/10.1073/pnas.012516899.

(26) Pilhofer, M.; Ladinsky, M. S.; McDowall, A. W.; Petroni, G.; Jensen, G. J. Microtubules in Bacteria: Ancient Tubulins Build a Five-Protofilament Homolog of the Eukaryotic Cytoskeleton. *PLoS Biol.* **2011**, *9* (12), e1001213. https://doi.org/10.1371/journal.pbio.1001213.

(27) Rogne, P.; Rosselin, M.; Grundström, C.; Hedberg, C.; Sauer, U. H.; Wolf-Watz, M. Molecular Mechanism of ATP versus GTP Selectivity of Adenylate Kinase. *Proc. Natl. Acad. Sci.* **2018**, *115* (12), 3012–3017. https://doi.org/10.1073/pnas.1721508115.

(28) Davis, C. M.; Gruebele, M. Cellular Sticking Can Strongly Reduce Complex Binding by Speeding Dissociation. *J. Phys. Chem. B* **2021**, *125* (15), 3815–3823. https://doi.org/10.1021/acs.jpcb.1c00950.

(29) Sukenik, S.; Ren, P.; Gruebele, M. Weak Protein-Protein Interactions in Live Cells Are Quantified by Cell-Volume Modulation. *Proc. Natl. Acad. Sci. U. S. A.* **2017**, *114* (26), 6776–6781. https://doi.org/10.1073/pnas.1700818114.

(30) McConkey, E. H. Molecular Evolution, Intracellular Organization, and the Quinary Structure of Proteins. *Proc. Natl. Acad. Sci. U. S. A.* **1982**, *79* (10), 3236–3240. https://doi.org/10.1073/pnas.79.10.3236.

(31) Wirth, A. J.; Gruebele, M. Quinary Protein Structure and the Consequences of Crowding in Living Cells: Leaving the Test-Tube behind: Prospects & Overviews. *BioEssays* **2013**, *35* (11), 984–993. https://doi.org/10.1002/bies.201300080.

(32) Martin-Galiano, A. J.; Oliva, M. A.; Sanz, L.; Bhattacharyya, A.; Serna, M.; Yebenes, H.; Valpuesta, J. M.; Andreu, J. M. Bacterial Tubulin Distinct Loop Sequences and Primitive Assembly Properties Support Its Origin from a Eukaryotic Tubulin Ancestor. *J. Biol. Chem.* **2011**, *286* (22), 19789–19803. https://doi.org/10.1074/jbc.M111.230094.

(33) Sarkar, M.; Li, C.; Pielak, G. J. Soft Interactions and Crowding. *Biophys. Rev.* **2013**, *5* (2), 187–194. https://doi.org/10.1007/s12551-013-0104-4.

(34) Guin, D.; Gruebele, M. Weak Chemical Interactions That Drive Protein Evolution: Crowding, Sticking, and Quinary Structure in Folding and Function. *Chem. Rev.* **2019**, *119* (18), 10691–10717. https://doi.org/10.1021/acs.chemrev.8b00753.

(35) Ranganathan, V. T.; Bazmi, S.; Wallin, S.; Liu, Y.; Yethiraj, A. Is Ficoll a Colloid or Polymer? A Multitechnique Study of a Prototypical Excluded-Volume Macromolecular Crowder. *Macromolecules* **2022**, *55* (20), 9103–9112. https://doi.org/10.1021/acs.macromol.2c00677.

(36) Denos, S.; Dhar, A.; Gruebele, M. Crowding Effects on the Small, Fast-Folding Protein Λ6-85. *Faraday Discuss.* **2012**, *157*, 451–500.

(37) Skóra, T.; Vaghefikia, F.; Fitter, J.; Kondrat, S. Macromolecular Crowding: How Shape and Interactions Affect Diffusion. *J. Phys. Chem. B* **2020**, *124* (35), 7537–7543. https://doi.org/10.1021/acs.jpcb.0c04846.

(38) Biswas, S.; Kundu, J.; Mukherjee, S. K.; Chowdhury, P. K. Mixed Macromolecular Crowding: A Protein and Solvent Perspective. *ACS Omega* **2018**, *3* (4), 4316–4330. https://doi.org/10.1021/acsomega.7b01864.

(39) Ellis, R. J.; Minton, A. P. Join the Crowd. *Nature* **2003**, *425* (6953), 27–28. https://doi.org/10.1038/425027a.

(40) Zimmerman, S. B.; Trach, S. O. Estimation of Macromolecule Concentrations and Excluded Volume Effects for the Cytoplasm of Escherichia Coli. *J. Mol. Biol.* **1991**, *222* (3), 599–620. https://doi.org/10.1016/0022-2836(91)90499-V.

(41) Koch, B.; Sanchez, S.; Schmidt, C. K.; Swiersy, A.; Jackson, S. P.; Schmidt, O. G. Confinement and Deformation of Single Cells and Their Nuclei Inside Size-Adapted Microtubes. *Adv. Healthc. Mater.* **2014**, *3* (11), 1753–1758. https://doi.org/10.1002/adhm.201300678.

(42) Davis, C. M.; Deutsch, J.; Gruebele, M. An in Vitro Mimic of In-Cell Solvation for Protein Folding Studies. *Protein Sci.* **2020**, *29* (4), 1046–1054. https://doi.org/10.1002/pro.3833.

(43) Davis, C. M.; Gruebele, M. Non-Steric Interactions Predict the Trend and Steric Interactions the Offset of Protein Stability in Cells. *ChemPhysChem* **2018**, *19* (18), 2290–2294. https://doi.org/10.1002/cphc.201800534.

(44) Xu, T.; Vavylonis, D.; Tsai, F.-C.; Koenderink, G. H.; Nie, W.; Yusuf, E.; Lee, I.-J.; Wu, J.-Q.; Huang, X. SOAX: A Software for Quantification of 3D Biopolymer Networks. *Sci. Rep.* **2015**, *5* (1), 9081. https://doi.org/10.1038/srep09081.

(45) Wieczorek, G.; Zielenkiewicz, P. Influence of Macromolecular Crowding on Protein-Protein Association Rates—a Brownian Dynamics Study. *Biophys. J.* **2008**, *95* (11), 5030–5036. https://doi.org/10.1529/biophysj.108.136291.

(46) Stewart, C. J.; Olgenblum, G. I.; Propst, A.; Harries, D.; Pielak, G. J. Resolving the Enthalpy of Protein Stabilization by Macromolecular Crowding. *Protein Sci.* **2023**, *32* (3), e4573. https://doi.org/10.1002/pro.4573.

(47) Kocherginsky, N.; Gruebele, M. Thermodiffusion: The Physico-Chemical Mechanics View. *J. Chem. Phys.* **2021**, *154* (2), 024112. https://doi.org/10.1063/5.0028674.

(48) Liu, F.; Nakaema, M.; Gruebele, M. The Transition State Transit Time of WW Domain Folding Is Controlled by Energy Landscape Roughness. *J. Chem. Phys.* **2009**, *131* (19), 195101. https://doi.org/10.1063/1.3262489.

TOC Figure: